Instant and Persistent Hydrogen Production Using Nano High Entropy Catalyst

Nirmal Kumar[†1], Subramanian Nellaiappan[†2], Ritesh Kumar[†3], Kirtiman Deo Malviya[4], K. G. Pradeep[5], Abhishek K. Singh*[3], Sudhanshu Sharma*[2], Chandra Sekhar Tiwary*[2], Krishanu Biswas*[1]

[1]Department of Materials Science and Engineering, Indian Institute of Technology Kanpur, Kanpur INDIA, 208016

[2]Department of Materials Science and Engineering, Indian Institute of Technology Gandhinagar, Gandhinagar - 382355, INDIA

[3]Materials research center, Indian Institute of Science, Bangalore-560012, INDIA

[4]Departemnt of Materials Engineering, Indian Institute of Science, Bangalore-560012, INDIA

[5]Departemnt of Materials Science and Metallurgical Engineering, Indian Institute of Technology Madras, Chennai-600036, INDIA

† equal contribution

Abstract

Renewable harvesting clean and hydrogen energy using the benefits of novel multi-catalytic materials of high entropy alloy (HEA equimolar Cu-Ag-Au-Pt-Pd) from formic acid with minimum energy input has been achieved in the present investigation. The synthesis effect of pristine elements in the HEA drives the electro-oxidation reaction towards non-carbonaceous pathway. The atomistic simulation based on DFT rationalize the distinct lowering of the d-band center for the individual atoms in the HEA as compared to the pristine counterparts. This catalytic activity of the HEA has also been extended to methanol electro-oxidation to show the unique capability of the novel catalyst. The nanostructured HEA, properties using a combination of casting and cryomilling techniques can further be utilized as fuel cell anode in direct formic acid/methanol fuel cells (DFFE).

The multi-principal multicomponent alloys popularly known as High Entropy Alloys (HEAs), containing at least five elements (in equimolar or near equimolar ratio) have heralded a new area of materials design. It opens vast compositional space and provides access to unique functional properties. The mixing of different elements has widely been utilized as an effective means to improve various properties, especially physical, chemical and electronic[1, 2, 3]. Due to the high entropy of mixing stabilizes the HEAs with the simple crystal structure (FCC, BCC structure), and the inherent structural stability and the flexibility to tune the composition with the desired catalytic entities enthused us to design and explore these materials for heterogeneous catalysis. The electro-oxidation of formic acid is imperative for the development of direct formic acid fuel cells (DFAFC). Platinum (Pt) and palladium (Pd) are two widely used noble-metal electro catalysts for catalyzing the formic acid into CO_2 and H_2 for DFAFC [4, 5, 6].

There are two competing pathways for this catalytic electro-oxidation process, one of them is direct oxidation, and the other one is indirect oxidation via CO intermediate. Direct oxidation is highly looked for, but it is very difficult for any catalyst to match the high catalytic efficiency of Pt and Pd. Even though the efficiencies of Pt and Pd is high but it is not high enough for the industrial application. To improve the catalytic activity, strategies such as alloying of Pt by less reactive noble metals M (M= Cu, Ag, Au, Ru, etc.) has been adopted. Another approach is to engineer the shape of the catalyst to maximize the exposure of the chemically active facets[7, 8]. Recent research focuses on single atom catalysis as a new frontier in the area of heterogeneous catalysis. These catalyst are highly active and stable during reactions[9, 10]. The strong bonding between the single metal atoms and the corresponding anchoring sites on the support are the key reasons [10] for the unusual activity and stability. However, these catalysts always required the energy input (electrochemical potential) to catalyze the reaction.

In current work, five catalytically active metals; Cu, Ag, Au, Pt, and Pd are mixed in an equimolar ratio to develop a high entropy alloy (Figure 1(a)). The HEAs are prepared using a scalable strategy involving a combination of vacuum-melting followed by low-temperature grinding. In the controlled composition HEAs, the homogeneously mixed solid solution of these elements consists of a 'single atom catalyst' of Pt, stabilized by other elements. These HEAs are utilized for the formic acid electrooxidation, an alternative proposition to generate hydrogen. Unlike conventional Pt nanoparticles, the HEAs produces a significant amount of hydrogen instantly at zero biased (i.e. without energy input). As an extension, HEAs are also explored for methanol electrooxidation. To rationalize the high activity of MEAs from atomistic level, density functional theory (DFT) is used, which based on d-band center establishes the superior performance of HEAs, compared to the pristine transition metals.

Results and discussion

Figure 1(b) shows X-ray diffraction (XRD) patterns of HEAs, exhibiting a single phase (FCC, a = 0.8173 nm). No peak related to individual elements (i.e., Pt, Pd, Cu, Ag, and Au) is observed in the pattern, confirming alloying of these constituents. Further, these nanoparticles have been characterized using UV –visible spectroscopy to confirm the nature of nanoparticles. The UV-vis spectra (Figure 1(c)) reveals the presence of two distinct and strong SPR bands at λ_{max} = 213 and 224 nm for HEAs. The peak positions are distinctly different as compared to individual peaks of Pt, Pd, Au, Ag and Cu nanoparticles, which is in-line with XRD observation. The digital picture of a colloidal solution of HEAs in methanol is shown as inset of Figure 1(c). It is also evident that the HEAs nanoparticles were easily dispersible in the organic solvent. Figure 1(d) shows scanning electron micrograph in BSE mode of the melted HEAs, revealing dendritic morphology with uniform chemical composition. The elemental mapping (energy dispersive spectroscopy) using

SEM is shown in Figure 1(d), revealing homogeneously distribution of the elements. The XPS spectra of the HEAs are shown in Figure 1(e). The Pt(4f) core level shows two peaks at 71.1 ($Pt4f_{7/2}$) and 74.4 ($Pt4f_{5/2}$) eV similar to bulk Pt [11]. Au(4f) core level spectra show two peaks at 84.0 eV and 88.0 eV related to $Au(4f_{7/2})$ and $Au(4f_{5/2})$ respectively, which is again similar to bulk Au. In the same way binding energy (B.E.) of Pd, Cu confirms the pure metallic characteristic with binding energies similar to its bulk counterpart. Interestingly, in HEAs the B.E. for $Ag3d_{5/2}$ appears at 367.8 eV, which 0.4eV lower than metallic Ag. This phenomenon is consistent with bimetallic Au-Ag alloy. XPS spectra of Cu suggest the formation of CuO on the surface apart from Cu metal. The Figure 2(a) low magnification dark field HAADF (High angle annular dark field) micrograph of the HEAs covering several nanoparticles, revealing uniform size and composition. The inset shows the selected area diffraction pattern of the FCC phase. Figure 2(b) shows HAADF image of one HEAs nanoparticle and its irregular morphology with a uniform composition contrast. The EDS composition map of the particle reveals uniform composition distribution. The HRSTEM (High resolution scanning transmission electron microscopy) image in HAADF shows Z contrast, revealing the composition of the individual lattice. It clearly shows a homogeneous mixture of constituent elements. The result of the 3D APT analysis is shown in Figure 2(d). The elemental distribution for the constituent elements (Ag, Cu, Pt, Pd, and Au) in the specimen is automatically homogeneous, indicating the formation of homogeneous multicomponent alloy in the nanocrystalline form.

The electrocatalytic performance of HEAs is assessed by the formic acid electrooxidation in the neutral electrolyte (Figure 3b(i)). The onset of oxidation is 0.0 V with the current value of ~3.5 mA, in contrast to the Pt nanoparticles where the current is zero at 0.0 V (Figure S5a). In the case of HEAs, a well-defined oxidation peak at ~0.69 V with a current value of 4.27 mA is observed,

which is related to the oxidation of HCOOH. Similarly, in the reverse scan, an anodic peak at ~0.32 V with a current value of 2.89 mA is observed, which is also attributed to the HCOOH oxidation preceded by the surface reduction[12, 13]. The forward and reverse peak current ratio (i_f/i_t) in HEAs is 1.47, which is about 3.5 times higher than the conventional Pt nanoparticles (0.4). This confirms the major contribution from the direct pathway[12, 13, 14]. Chronoamperometry at 0.7 V for 1000 seconds in an air-tight cell is carried out to analyze the evolved gases (Figure 3b(ii)). As soon as the potential is applied, a large number of bubbles (Figure 3b (iii)) form instantaneously over HEAs (working electrode). The gaseous products formed are analyzed using GC. Surprisingly, an enormous amount of hydrogen (counter reaction product) forms, which is accompanied by CO_2 and a noticeable amount of CO (Figure S2c). It's important to note that, the free CO formation indicates that the formic acid oxidation mechanism must includes its contribution. Similar chronoamperometry experiment (Figure S5d) with Pt nanoparticles produces hydrogen with a higher amount of CO_2 and CO as compared to HEAs (S5f) (table 1).

In literature, the Pt-Ru alloy has been employed to enhance the activity of methanol and formic acid oxidation. It is stated that the presence of Ru enhances the OH adsorption and enhances the oxidation of CO to CO_2 [15]. One can anticipate the similar mechanism in the HEAs as well. However, experimentally the role of individual metallic species is difficult to pinpoint.

The formic acid oxidation even at 0.0 volts (Figure 3b(iv)) led to the conclusion that the catalyst possibly works under the unbiased condition as well. Therefore, the electro-oxidation under open circuit potential is carried out for 2000 seconds (Figure 3b(v)). After 2000 seconds, the gaseous products show the signals for hydrogen, CO_2, and CO (Figure S5a,b) proving that the HEAs has the ability to oxidize formic acid without any applied potential, whereas Pt nanoparticles does not show any detectable hydrogen (Figure S5c-e).

The similar catalytic activity for methanol is also demonstrated (Figure 3(a) (i)). The onset oxidation potential is ~0.27 V, and an intense peak at ~0.8 V is observed, which is attributed to the formation and oxidation of CH_3OH [15]. In the reverse (cathodic) scan, a minor anodic peak at 0.42 V appears due to the re-oxidation of methanol preceded by the reduction of the oxidized surface [14]. The ratio of forward peak current (i_f) to reverse peak current (i_r) of HEAs (i_f/i_r =4) is four times higher than the conventional Pt nanoparticles (i_f/i_r =1, Figure S4a) indicating that the HEAs catalyst follows direct oxidation pathways with very less CO formation. From the Table 1 it is clear that under all conditions HEAs catalyst outperforms the Pt nanoparticles in regards to hydrogen production. Importantly, the amount of CO produced in HEAs is comparatively lower than Pt nanoparticles, revealing the dominance of direct oxidation pathway both in methanol and formic acid oxidation. Figure 3(c)(i-iii) shows a comparison of gaseous product during the electrooxidation of methanol (Figure 3c(i)) and formic acid under biased (Figure 3c(ii)) and unbiased (Figure 3c(iii)) conditions. From this bar diagram, one can deduce the superior activity of HEAs compared to Pt nanoparticles. It is worth mentioning that this is the first observation for the electro-oxidation of formic acid in an unbiased condition and it paves the way to generate hydrogen gas from formic acid with a minimum input of energy and low CO and CO_2 formation. Based on the above experimental observations, it is difficult to pinpoint the catalytic role of individual constituent's elements in the multi-component HEAs. Therefore, to gain an insight of the process, we have performed DFT calculations. The electro-oxidation of Formic acid is chosen as a representative model reaction for the simulation. The catalytic activity of the HEAs is compared with all its pristine components. The optimized lattice parameters of Pt are, a = b = c = 3.92 Å, which is in excellent agreement with previous reports. The most stable facets in FCC metals, i.e., the (111) facets were chosen for calculations. All the (111) facets of pristine metals –

Pt, Pd, Ag, Au, and Cu were analyzed with the same supercell size as that of the HEAs. The unit-cell of HEAs contained 120 atoms, with 20% each of Pt, Pd, Ag, Au and Cu atoms of the total composition.

To make an estimate of the activity of HEAs and the pristine metal surfaces, their d-band centers were calculated, as they are important descriptors of the catalytic activity. The activity of formic acid decomposition has also been found related to the d-band center of the metal under consideration [16]. The experimentally observed increase in activity of HEAs can be explained from Figure 4, where the d-band centers of HEAs have been compared with all pristine metal (111) surfaces. The d-band centers of all components except Au (in which d-band centers remain the same) become closer to the fermi-level, leading to the increase in activity.

Subsequently, the formic acid (HCOOH) decomposition was performed on pristine Pt (111) and HEAs surface. The adsorption of the key intermediate (formate (HCOO*)) on both surfaces were checked. Only Pt and Pd atoms were chosen as they were found to be most active among all five metals from the d-band center analysis. Furthermore, the electron localization function (ELF) plots (Figure. 4(c) & (d)), show that electron is completely localized on H, in both cases, which indicates the formation of H- upon dissociation of HCOO*. The ELF plots show comparatively more localization of electrons on two oxygen atoms in the case of HCOO* adsorbed on alloy surface than on pristine Pt (111) surface. This leads to weaker bonds between O and the metal atoms (Pt and Pd) on alloy surface than that on the pristine surface. Hence, the decomposition of formate will be easier on the HEAs surface compared to the pristine Pt surface. Also, HCOO* intermediate is found to be symmetrically adsorbed (Figure 4(c)) on pristine Pt (111) surface, while on HEAs, it is asymmetrically adsorbed (Figure 4(d)). This gives another indication of difference in the mechanism of formic acid decomposition on two surfaces. While on pristine Pt (111), both Pt-O

bond dissociates simultaneously to form CO_2 and H_2, on the other hand in the case of HEAs, first Pd-O bond dissociation followed by Pt-O bond.

Based on experimental and theoretical understanding, we attribute the superior catalytic performance of HEAs (Cu-Ag-Au-Pt-Pd alloy) to the synergism between the metals. The remarkable electrocatalytic activity of HEAs in unbiased condition (zero potential) and apparent surface poisoning tolerance towards carbonaceous species are superior to the Pt nanoparticles. Instantaneous production of high amount of hydrogen at unbiased condition makes HEAs an active catalyst for hydrogen production from formic acid.

Conclusion

In conclusion, we demonstrated an easily scalable processing technique to produce compositionally controlled nanocrystalline equi-atomic Cu-Ag-Au-Pd-Pt, HEAs. The macroscopic and microscopic techniques have been utilized to reveal the atomic distribution in the homogenous mixed HEAs. The synergistic effect of individual metal component results in higher catalytic activity towards formic acid electro-oxidation. The unique instant catalytic activity is shown by dissociating formic acid into hydrogen under zero biased (zero energy input) condition. The amount of carbonaceous gases are surprisingly low with HEAs proving the preferred direct oxidation pathway. The density functional theory (DFT) study establish the HEAs as a superior catalyst, compared to the pristine transition metals, on the basis of d-band center theory. It also gives a clue of difference in the mechanism of formic acid electro-oxidation on HEAs surface with respect to the pristine Pt. The current findings are extended to methanol electro-oxidation, where a similar high activity is attained. The current finding can be utilized to develop direct formic acid/methanol fuel cells (DFFC) for green energy generation also harnessing hydrogen from these fuels.

Acknowledgments: Author would like to thanks Department of Science and Technology India. RK and AKS acknowledge Materials Research Centre, Thematic Unit of Excellence, and Supercomputer Education and Research Centre for providing the computing facilities.

Competing interests

The authors declare no competing interests

Authors contribution

NK, SN, SS, CST, KB participated in experiments and RK and AKS performed simulation. KDM and KGP performed microscopy and atom probe. All author participated in analysis and writing manuscript.

Materials and Methods

The elements granules (Cu, Ag, Au, Pt, Pd) were purchased from Alfa Aesar, USA, with the purity 99.9 at% and used for preparation of high entropy alloys (Cu-Ag-Au-Pt-Pd) ingot. This was prepared in the high purity argon atmosphere utilizing arc melting. Further, ingot homogenized at 1000 ^{o}C for 12 hours to acquire large grains and strong chemical homogeneity. These ingots were pulverized in a liquid nitrogen cooled (at-160±10 ^{o}C) cryomill[17] consisting of 5cm diameter single ball (tungsten carbide). The extra precautions have been taken during milling by purging argon (Ar) gas, which further protects the powder from oxidation. After six hours of cryomilling, the HEAs-NPs (cryomilled powder) were collected for characterizations.

The morphology, size of the HEA nanoparticles have been characterized using Transmission electron microscope (FEI TITAN and Technai G^2, UT 20 operated at 300 and 200 kV respectively). The chemical composition of the nanoparticle has been estimated using energy dispersive spectroscopic detectors (known Super EDS) attached to TITAN. The elemental mapping signifying distribution of elements in the nanoparticles was obtained using Super EDS detectors. Atomic scale distribution of atoms in the alloy was obtained using three-dimensional atom probe tomography in a local electrode atom probe (LEAP 4000X HRTM, Cameca Instruments, France). APT measurement was performed in laser pulsing mode using 30 pJ laser energy at 250 kHz repetition rates, while the tip was maintained at 60 K. Needle shaped specimens for APT was prepared from the samples using a dual beam, Helios Nanolab 660 focused ion beam work station. Reconstruction and analysis of the APT data were carried out using IVAS 3.6.10a software (Cameca Instruments, France). The chemical structure determination has been studied using X-ray photoelectron spectroscopy (XPS, PHI5000, Versa Prob II, FEI Inc.). The XPS peaks charge correction has been made using adventitious carbon (284.6 eV) and the spectral peaks deconvolution have been performed using CASA XPS software. Further, the compositions of the as cast ingot and nanoparticles were determine using electron probe micro analyzer (EPMA- JXA-8230; JEOL, Japan).

The conventional three-electrode system (CHI408C electrochemical workstation) has been used for electrochemical studies. The working electrode was made by mixing 100 mg of catalyst and binder (200 µL of 5% Nafion solution). The isopropanol was added to it to make thin slurry, which is deposited on a glassy carbon electrode (GCE). Platinum wire was used as the counter electrode, and Ag/AgCl electrode was used as the reference electrode. Supporting electrolyte solutions are KNO_3 (0.5 M) for methanol oxidation and K_2SO_4 (0.5 M) for formic acid oxidation reactions. For cyclic voltammetry (CV) experiments, 500 µL of respective analysts were taken and made up to 10 mL using respective supporting electrolytes. An air-tight electrochemical cell was used for the

product formation and analysis. For gaseous products analysis, a gas-tight syringe (1 mL) was used to transfer the evolved gases into gas chromatograph (GC: CIC Baroda) using a TCD (thermal conductivity detector) () for detecting H_2 and FID (flame ionization detectors) for detecting CO and CO_2. A standard gas mixture was used for calibrating the GC.

Computational Methodology

First principles calculations were performed using density functional theory (DFT) as implemented in the Vienna ab-initio simulation (VASP 5.4.1) package[18]. The interactions between electrons and ions were described using all-electron projector augmented wave (PAW) pseudopotentials. The electronic exchange and correlations were approximated by Perdew-Burke-Ernzerhof (PBE) under generalized gradient approximation (GGA)[19]. The optimization of all structures were performed using a conjugate gradient scheme until the convergence criteria for energies and the forces reached 10^{-5} eV and 0.01 eV Å-1, respectively. All (111) surfaces of Pt, Pd, Ag, Au and Cu were generated from their optimized bulk structures using Virtual NanoLab version 2016.2. The Cu-Ag-Au-Pt-Pd alloy (HEAs) structure was generated from 5x3x1 supercell of Pt (111) surface using the ATAT code. The structure had 3 layers of atoms with the bottom two layers frozen and allowing only the topmost layer to relax, to mimic the bulk behavior.

Figure

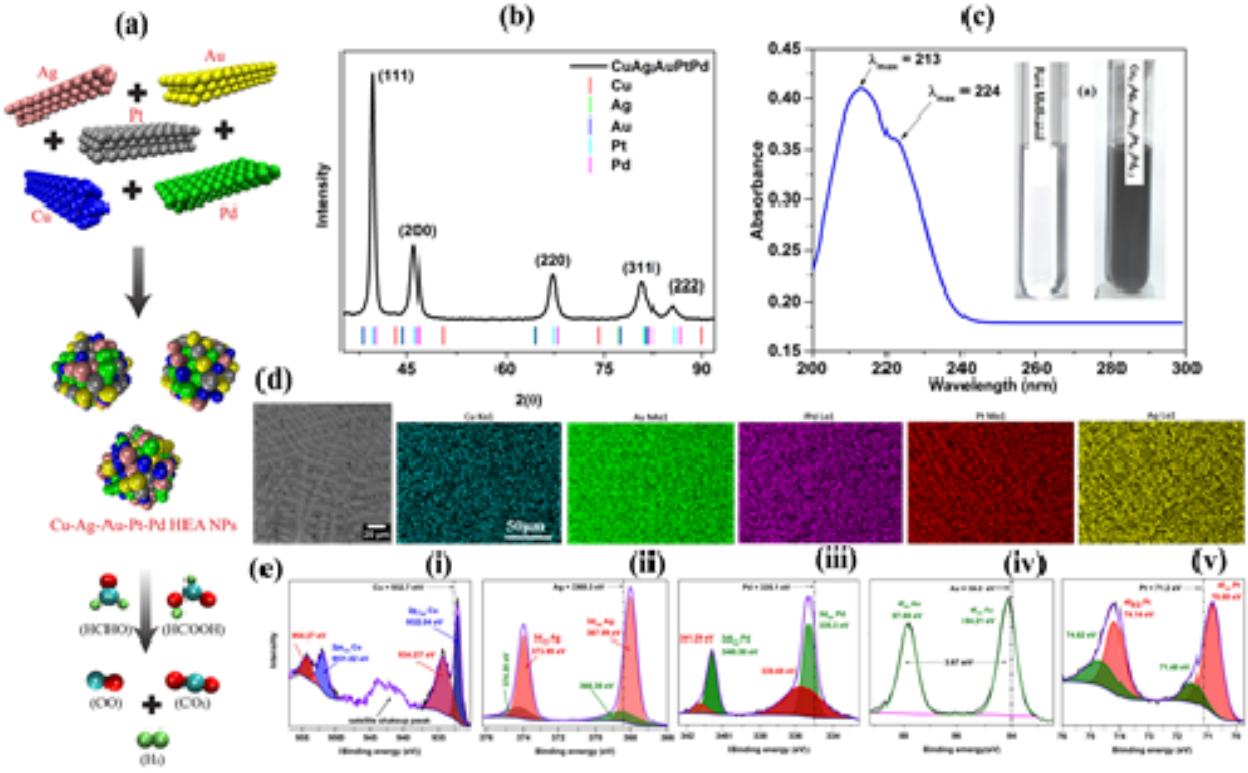

Figure.1: Materials Characterization of HEAs: (a) Schematics of HEA nanoparticle preparation and its activity; (b) X-ray diffraction pattern of Cu-Ag-Au-Pt-Pd (ingot) as well as nanoparticles (inset shows (111) peak broadening); (c) UV absorbance spectra of nanoparticles dispersed in pure methanol; (d) BSE image of ingot surface (e) SEM-EDAX elemental mapping of ingot surface; (f) X-ray photoelectron spectroscopy spectra of prepared Cu-Ag-Au-Pt-Pd nanoparticles.

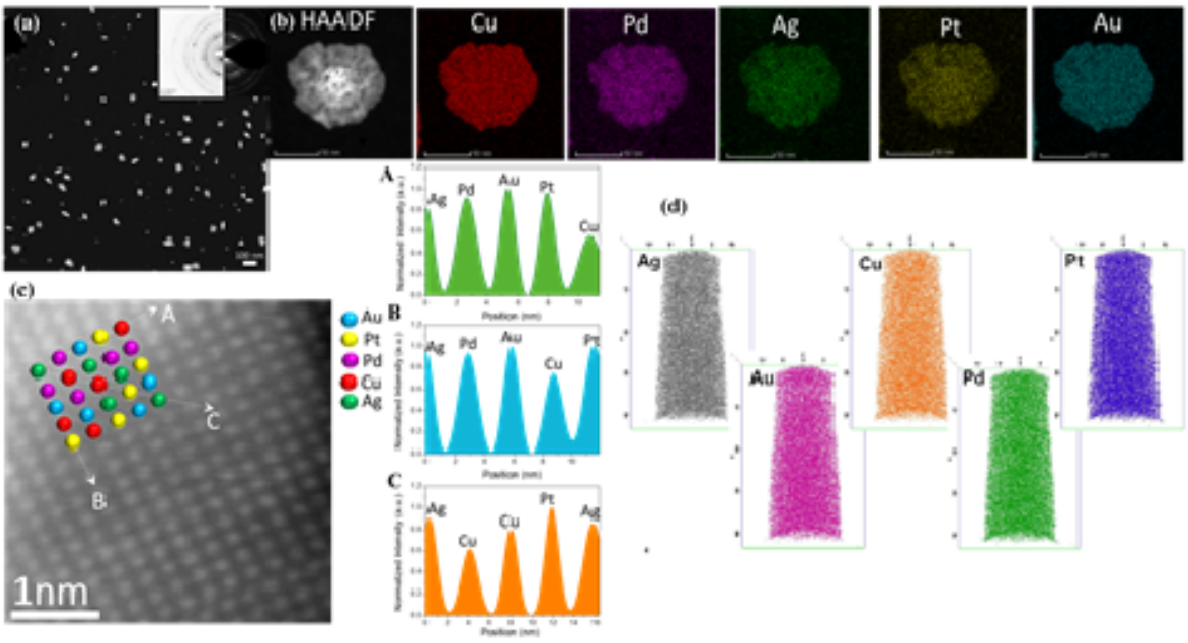

Figure.2: Composition analysis of HEAs: (a) Low magnification darkfield image with large number of particles, inset shows selected area diffraction covering several particles, revealing 111, 200, 220, 311 and 222 reflections. (b) HAADF image of single particle and composition map of the particle. (c) HRSTEM image in HAADF mode of an edge of particle, marked with different intensity **(d)** three-dimensional elemental distribution of atom probe (elements are marked).

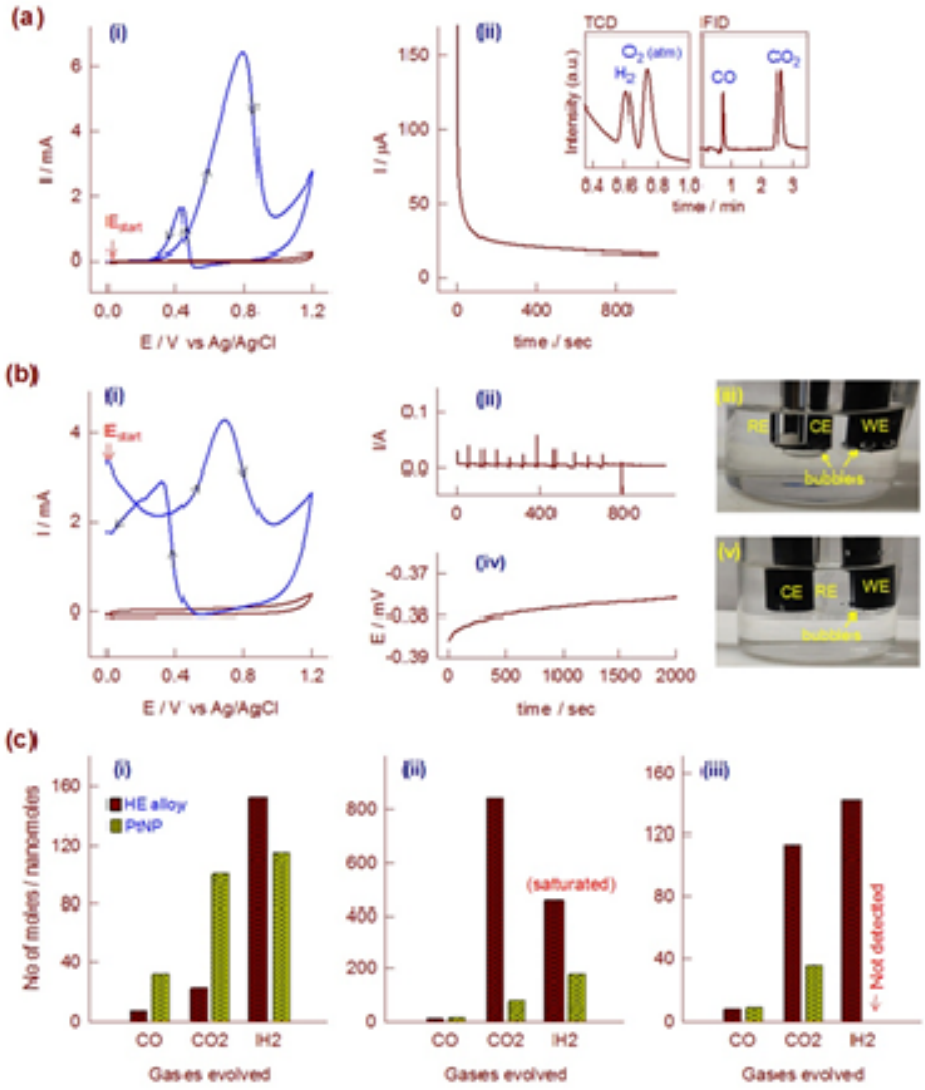

Figure.3: Hydrogen evaluation of HEAs:(a) Cyclic voltammetric responses of (i) HEAs deposited on glassy carbon electrode for the electro-oxidation of 500 µL methanol at a scan rate of 20 mV s^{-1} and (ii) chrono-amperometric response of methanol at a fixed potential of 0.8V for 1000 sec along with gas chromatography TCD and FID signals in 0.5 M KNO_3 electrolyte. **(b)** Cyclic voltammetric responses of (i) HEAs deposited on the glassy carbon electrode for the electro-oxidation of 500 µL formic acid at a scan rate of 20 mV s^{-1} and (ii) its chrono-amperometric response at a fixed potential of 0.7V for 1000 sec, (iv) open circuit potential (unbiased) for 2000 sec in 0.5 M K_2SO_4 electrolyte. Images are taken during their respective experiments (iii and v). **(c)** Comparative bar diagrams for the number of moles of gases evolved and detected during methanol oxidation at 0.8 V (i) and formic acid at biased (ii) and unbiased (iii) conditions such as CO, CO_2, H_2 by gas chromatography on HEAs and Pt nano catalyst deposited glassy carbon electrode.

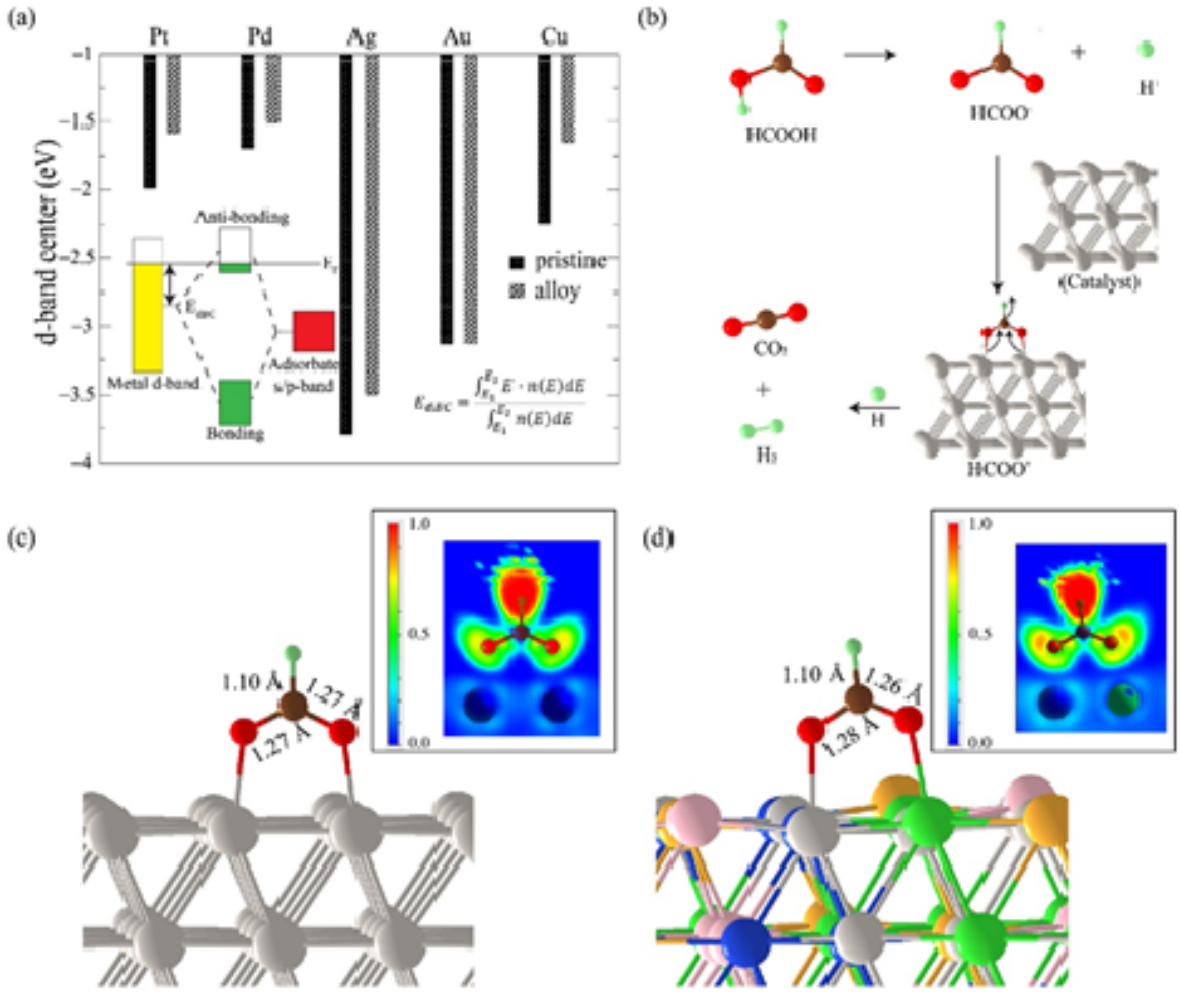

Figure.4: Simulation of hydrogen evaluation of HEAs: ***(a)*** Position of d-band centers (E_{dBC}) of components of alloy Cu-Ag-Au-Pt-Pd, compared with their pristine Pt (111) surfaces' values. E_{dBC} is defined as the first moment of density of d-states (inset in right). E and n(E) are the energies and corresponding densities of d-band. E_1 and E_2 are the energy range of d-states. The inset in the left shows how E_{dBC} affects catalytic activity. If E_{dBC} lies closer to the fermi level (E_F), then the antibonding metal-adsorbate state will be filled to lesser extent, thereby stabilizing the metal-adsorbate interactions. ***(b)*** Schematic of formic acid (HCOOH) decomposition on catalyst surfaces. At first, HCOOH ionizes to form formate ion and proton. The formate ion then adsorbs on the catalyst surface in a bidentate fashion when CO_2 is released (*20*). Structures of HCOO optimized on ***(c)*** pristine Pt (111) and on ***(d)*** the CuAgAuPtPd alloy. The inset on the right shows plots for electron localization function (ELF) (*16*) for the respective systems. The value of ELF lies between 0 and 1, where 0, 0.5 and 1 represents absence of electrons, uniform electron gas and localization of electrons, respectively. Grey, green, pink, yellow, violet, red, brown and lime colored spheres represent Pt, Pd, Ag, Au, Cu, O, C and H atoms, respectively. The two C-O bonds in formic acid are 1.35 (single bonded) and 1.21 (double bonded) Å, respectively. This indicates partial double bond character in both C-O bonds in HCOO*.

References and Notes:

1. Miracle DB, Senkov ON. A critical review of high entropy alloys and related concepts. *Acta mater* **122**, 448-511 (2017).

2. Ye YF, Wang Q, Lu J, Liu CT, Yang Y. High-entropy alloy: challenges and prospects. *Materials Today* **19**, 349-362 (2016).

3. Gludovatz B, Hohenwarter A, Catoor D, Chang EH, George EP, Ritchie RO. A fracture-resistant high-entropy alloy for cryogenic applications. *Science* **345**, 1153-1158 (2014).

4. Marcinkowski MD, *et al.* Selective Formic Acid Dehydrogenation on Pt-Cu Single-Atom Alloys. *ACS Catal* **7**, 413-420 (2017).

5. Sheng Z, Yuyan S, Geping Y, Yuehe L. Electrostatic Self-Assembly of a Pt-around-Au Nanocomposite with High Activity towards Formic Acid Oxidation. *Angew Chem Int Ed* **49**, 2211-2214 (2010).

6. Iyyamperumal R, Zhang L, Henkelman G, Crooks RM. Efficient Electrocatalytic Oxidation of Formic Acid Using Au@Pt Dendrimer-Encapsulated Nanoparticles. *J Am Chem Soc* **135**, 5521-5524 (2013).

7. Yin A-X, Min X-Q, Zhang Y-W, Yan C-H. Shape-Selective Synthesis and Facet-Dependent Enhanced Electrocatalytic Activity and Durability of Monodisperse Sub-10 nm Pt–Pd Tetrahedrons and Cubes. *J Am Chem Soc* **133**, 3816-3819 (2011).

8. Liu H, *et al.* Hollow and Cage-Bell Structured Nanomaterials of Noble Metals. *J Am Chem Soc* **134**, 11602-11610 (2012).

9. Chengzhou Z, Shaofang F, Qiurong S, Dan D, Yuehe L. Single-Atom Electrocatalysts. *Angew Chem Int Ed* **56**, 13944-13960 (2017).

10. Jiwhan K, *et al.* Highly Durable Platinum Single-Atom Alloy Catalyst for Electrochemical Reactions. *Adv Energy Mater* **8**, 1701476 (2018).

11. Shyu JZ, Otto K. Identification of platinum phases on γ-alumina by XPS. *Appl Surf Sci* **32**, 246-252 (1988).

12. Gao W, Keith JA, Anton J, Jacob T. Theoretical Elucidation of the Competitive Electro-oxidation Mechanisms of Formic Acid on Pt(111). *J Am Chem Soc* **132**, 18377-18385 (2010).

13. Bisht A, Zhang P, Shivakumara C, Sharma S. Pt-Doped and Pt-Supported La1–xSrxCoO3: Comparative Activity of Pt4+ and Pt0 Toward the CO Poisoning Effect in Formic Acid and Methanol Electro-oxidation. *J Phys Chem C* **119**, 14126-14134 (2015).

14. Huang W, *et al.* Highly active and durable methanol oxidation electrocatalyst based on the synergy of platinum-nickel hydroxide-graphene. *Nat Commun* **6**, 10035 (2015).

15. Iwasita T, Hoster H, John-Anacker A, Lin WF, Vielstich W. Methanol oxidation on PtRu electrodes. Influence of surface structure and Pt-Ru atom distribution. *Langmuir* **16**, 522-529 (2000).

16. Tedsree K, *et al.* Hydrogen production from formic acid decomposition at room temperature using a Ag-Pd core-shell nanocatalyst. *Nat Nanotechnol* **6**, 302-307 (2011).

17. Kumar N, Biswas K. Fabrication of novel cryomill for synthesis of high purity metallic nanoparticles. *Rev Sci Instrum* **86**, 083903-083908 (2015).

18. Kresse G, Hafner J. Ab initio molecular dynamics for liquid metals. *Physical Review B* **47**, 558-561 (1993).

19. Perdew JP, Burke K, Ernzerhof M. Generalized Gradient Approximation Made Simple. *Phys Rev Lett* **77**, 3865-3868 (1996).

20. Tedsree K, Kong ATS, Tsang SC. Formate as a surface probe for ruthenium nanoparticles in solution 13C NMR spectroscopy. *Angew Chem Int Ed* **48**, 1443-1446 (2009).

Table 1:

Gases detected in GC	Number of moles of gases evolved and detected (nanomoles)					
	HEAs			Pt nanoparticles		
	Methanol	Formic acid		Methanol	Formic acid	
	Biased @ 0.8V	Biased @ 0.7V	Un-biased (OCP)	Biased @ 0.8V	Biased @ 0.7V	Un-biased (OCP)
H_2	152.17	saturated	142.61	117.16	176.08	N.D
CO_2	23.95	84.29	113.89	102.56	82.16	35.77
CO	7.58	12.79	8.48	31.63	15.36	9.34